A ventilation-based framework to explain the regeneration-scavenging balance of iron in the ocean

Alessandro Tagliabue[1], Richard G. Williams[1], Nicholas Rogan[1], Eric P. Achterberg[2], and Philip W. Boyd[3]

[1]Department of Earth, Ocean and Ecological Sciences, School of Environmental Sciences, University of Liverpool, Liverpool, UK, [2]GEOMAR Helmholtz Centre for Ocean Research Kiel, Kiel, Germany, [3]Institute for Marine and Antarctic Studies, University of Tasmania, Hobart, Tasmania, Australia

Abstract Our understanding of the processes driving the patterns of dissolved iron (DFe) in the ocean interior, either in observations or models, is complicated by the combined influences of subduction from the surface mixed layer, notable subsurface sources, regeneration, and scavenging loss. We describe a ventilation-based framework to quantify these processes in a global ocean biogeochemical model including diagnostics along potential density surfaces. There is a prevailing control of subsurface DFe by the subduction of surface DFe as preformed DFe augmented by benthic sources of DFe from hydrothermal activity and sediments. Unlike phosphate, there is often a first-order balance with a near cancelation between regeneration and scavenging with the remaining "net regeneration" controlled by the ventilation of surface excesses in Fe-binding ligands. This DFe framework provides a more stringent test of how the total DFe distribution is mechanistically controlled within a model and may be subsequently used to interpret observed DFe distributions.

1. Introduction

Dissolved iron (DFe) is considered to be the limiting nutrient for phytoplankton growth across the Southern Ocean and over parts of the Pacific and Atlantic Oceans [*Boyd and Ellwood*, 2010; *Moore et al.*, 2013]. Accordingly, rates of primary production and nitrogen fixation, as well as their sensitivity to change, are underpinned by fluctuations in DFe availability [*Schlosser et al.*, 2013; *Tagliabue et al.*, 2014a]. Dissolved Fe is supplied to surface-dwelling phytoplankton from above via dust deposition [*Jickells et al.*, 2005] or from below by vertical mixing or upwelling of subsurface DFe [*Tagliabue et al.*, 2014b]. Synthesis studies suggest that these subsurface DFe pools dominate supply over most of the DFe-limited regions, such as the Southern Ocean [*Boyd et al.*, 2012; *Tagliabue et al.*, 2010].

Due to its short residence time of a few decades, the subsurface DFe distribution might be expected to closely resemble local sources associated with organic matter remineralization [*Boyd et al.*, 2010] and the direct DFe input from sediments and hydrothermal vents [*Tagliabue et al.*, 2010]. However, this local source-driven viewpoint might be significantly modified by ocean transport and mixing, such as the subduction of unutilized surface water DFe noted in some studies [*Ussher et al.*, 2013] that spreads preferentially along potential density surfaces.

In order to unravel questions of how the distributions of trace metals are controlled, the observational coverage for DFe has expanded markedly during the GEOTRACES program (www.geotraces.org), providing full depth sections with many thousands of DFe measurements. These data sets provide important constraints on ocean biogeochemical models that seek to represent the oceanic DFe cycle. In this regard, it is challenging to understand how the DFe distribution is controlled by the interplay of subduction, transport from hydrothermal and sediment sources in the ocean interior, and the DFe supply from remineralization and/or removal by scavenging. For example, a model may arrive at a given DFe concentration via a range of different processes—as noted for phosphate (PO_4) [*Duteil et al.*, 2012]. The preformed/regenerated framework suggests that around half of the total ocean PO_4 is associated with regeneration [*Duteil et al.*, 2012; *Ito and Follows*, 2005], and there have been similar efforts to diagnose DFe regeneration [*Fitzsimmons et al.*, 2013; *Rijkenberg et al.*, 2012]. However, the signal of DFe regeneration is affected by losses due to scavenging and additional subsurface inputs from sediments and hydrothermal vents, so the partitioning of DFe is more complex than for PO_4.

In this study, we describe a DFe framework that separates the interior ocean DFe pool into its constituent parts in order to understand how the DFe distribution is controlled. This new framework is applied to the state of the art NEMO-PISCES ocean general circulation and biogeochemistry model, which is widely used for global DFe studies [*Tagliabue et al.*, 2014a, 2010]. Our framework builds on similar ideas developed for PO_4 [*Ito and Follows*, 2005] but is expanded to account for the additional complexities of the DFe cycle. We use this framework to explore the different roles for each component across the Atlantic and Pacific Oceans and highlight an important role for ventilation in governing the DFe distribution and, in particular, the balance between regeneration and scavenging of DFe.

2. A Preformed Iron Framework

2.1. Theory

In the ocean interior, total DFe (DFe_{TOT}) can be made up of (i) an unused preformed (DFe_{PRE}) pool subducted from the ocean surface mixed layer, (ii) DFe supplied from sediments (DFe_{SED}) and hydrothermal vents (DFe_{HYD}), (iii) DFe regenerated from sinking organic matter (DFe_{REG}), and (iv) a scavenged component (DFe_{SCAV}) that removes DFe:

$$DFe_{TOT} = DFe_{PRE} + DFe_{SED} + DFe_{HYD} + DFe_{REG} - DFe_{SCAV}. \tag{1}$$

This framework differs from the simpler balance often implemented for PO_4 [*Ito and Follows*, 2005] that separates PO_4 into contributions from preformed (P_{PRE}) and regenerated (P_{REG}) components. However, the DFe distribution cannot be understood from the simpler PO_4 balance without taking into account (as in equation (1)) the effects of subsurface DFe sources, variable Fe/O_2 ratios, and DFe scavenging on the ocean DFe cycle [*Boyd and Ellwood*, 2010]. An additional difficulty is that DFe_{REG} is a function of apparent oxygen utilization (AOU) and the Fe/O_2 ratio, but this regenerated component varies widely due to Fe/O_2 ratios being more variable than P/O_2 ratios [*Strzepek et al.*, 2012].

2.2. Implementation Into NEMO-PISCES

NEMO-PISCES was modified to explicitly simulate DFe_{PRE}, DFe_{HYD}, and DFe_{SED}, along with DFe_{TOT}, as prognostic tracers, with DFe_{REG} computed by the model and DFe_{SCAV} determined as a residual from equation (1). By definition, DFe_{PRE} is set equal to DFe_{TOT} within the surface mixed layer and then transported by the ocean circulation until DFe_{PRE} is returned to the surface mixed layer and reinitialized to DFe_{TOT}. Since NEMO-PISCES considers inputs of DFe from sediments and hydrothermal vents [*Tagliabue et al.*, 2014a], DFe_{SED} and DFe_{HYD} are initialized in grid cells where sediment and hydrothermal supply is active. In those grid cells, DFe_{PRE} is first subtracted from DFe_{TOT} to avoid erroneously counting this fraction as a benthic source, with DFe_{SED} or DFe_{HYD} then set equal to $DFe_{TOT} - DFe_{PRE}$. Where there is dual input of DFe from sediments and hydrothermal vents, the allocation to DFe_{SED} and DFe_{HYD} is adjusted by the relative strength of each source. By definition, DFe_{SED} and DFe_{HYD} are set to zero when they upwell into the surface mixed layer. After being initialized, DFe_{PRE}, DFe_{SED}, and DFe_{HYD} are transported by the ocean circulation and not altered until they reencounter these specific conditions (within the surface mixed layer or adjacent to benthic sources). We note that while NEMO-PISCES considers dust deposition of DFe [*Tagliabue et al.*, 2014a], this process supplies Fe to surface waters and is thus accounted for within DFe_{PRE}. DFe_{REG} is computed from the modeled AOU, the dynamic Fe/C ratio ($R_{Fe:C}$) present in the model (ranging between 1 and 40 µmol:mol), and the prescribed model O_2/C ratio of 133/122 mol:mol. Thus, DFe_{REG} varies in space and time as a function of AOU (a function of temperature and O_2) and $R_{Fe:C}$ (a function of DFe_{TOT} at first order). After initializing DFe_{PRE}, DFe_{SED}, and DFe_{HYD} as zero, we ran simulations of 3000 years under seasonally repeating physical forcing by which time any drift in the tracers was negligible.

NEMO-PISCES has a resolution of 2° by 2° cos (latitude) with the resolution enhanced to 0.5° at the equator. The model has 30 vertical levels, with an increment that increases from 10 m at the surface to 500 m at depth (12 levels are located in the first 125 m). For this study we used the "INCA" dust deposition field and more information on the Fe cycle and statistics related to the modeled DFe fields is available in *Tagliabue et al.* [2014a]. Our model does not discriminate between "new" sedimentary DFe and DFe that was regenerated *within* the sediments and released to the overlying water column. Alternatively, DFe_{SED} and DFe_{HYD} could be linked to the fluxes of DFe associated with each source, but since some of this flux will be lost via local scavenging, we chose to quantify the overall impact on DFe concentrations.

3. Interpretation of the Modeled Distribution of Dissolved Iron

3.1. The Preformed Imprint on Dissolved Iron

Overall, there is an important role for ventilation in controlling the distribution of DFe_{TOT} with a dominant contribution of DFe_{PRE} over large parts of the Atlantic and Pacific Oceans. The strong underlying influence of ocean ventilation and transport on DFe distributions is revealed by the generally close correspondence between DFe_{PRE} (our ventilated DFe tracer) and DFe_{TOT}. The basin mean DFe_{TOT} and DFe_{PRE} are similar in the well-ventilated Atlantic, with DFe_{PRE} averaging 0.56 ± 0.15 nM compared to 0.57 ± 0.10 nM for DFe_{TOT} (Figure 1). However, DFe_{TOT} and DFe_{PRE} are relatively uncoupled in the less well ventilated Pacific, where DFe_{PRE} tends to be lower than DFe_{TOT} (0.47 ± 0.14 and 0.58 ± 0.14 nM, respectively, Figure 2). The increasing DFe_{TOT} concentrations toward the Northern latitudes of the Atlantic are linked to DFe_{PRE}, while the subduction and northward expansion of low DFe_{PRE} at more southerly latitudes is mirrored in lower thermocline DFe_{TOT} (Figures 1a and 1b). In both cases, this distribution is due to the ventilation and transport of surface DFe as DFe_{PRE} and highlights the far-field influence of surface DFe concentrations in the ocean interior. Despite the importance of the subduction of low DFe_{PRE} in the South Pacific, DFe_{PRE} remains a smaller component of DFe_{TOT} across the Pacific basin (Figures 2a and 2b), likely due to the lesser levels of ventilation in this basin.

The contribution of DFe_{PRE} is more clearly appraised along potential density surfaces that reflect the spreading of mode waters, rather than along discrete depths. To illustrate this ventilated connection, we consider the $\sigma_\theta = 26.2$ surface for lighter subtropical mode waters, $\sigma_\theta = 27.2$ surface for denser subtropical/subpolar mode waters, and $\sigma_2 = 36.9$ surface for intermediate/deep waters [*Hanawa and Talley*, 2001; *Talley*, 1999] averaged over the Atlantic and Pacific basins (Figure 3); σ_θ and σ_2 are the potential densities minus $1000 \, kg \, m^{-3}$ referenced to the sea surface or a depth of 2 km, respectively. The pattern of ventilation varies dramatically from $\sigma_\theta = 26.2$ to 27.2 [*Talley*, 1999; *Williams and Follows*, 2011]: for the lighter surface, ventilation occurs at mid and high latitudes in each basin, while for the denser surface, the ventilation occurs from the mid and high latitudes of the North Atlantic and Southern Ocean, but not for the North Pacific. For the intermediate and deep waters, the ventilation is only from the high latitudes of the North Atlantic and Southern Ocean.

In the well-ventilated Atlantic, along the $\sigma_\theta = 26.2$ surface, DFe_{PRE} is dominant at northern latitudes with a declining influence farther south (Figure 3a). For the denser $\sigma_\theta = 27.2$ surface, there is a greater mismatch between DFe_{TOT} and DFe_{PRE} away from the northern and southern outcrops in the basin (Figure 3b). For intermediate and deep waters along the $\sigma_2 = 36.9$ surface, DFe_{TOT} and DFe_{PRE} remain tightly connected, with DFe_{PRE} switching from being slightly greater than DFe_{TOT} to slightly less from north to south (Figure 3c). For the less well ventilated Pacific, DFe_{PRE} underestimates DFe_{TOT} (even on the lightest mode water surface), apart from at the northern and southern outcrops (Figure 3d). This pattern persists along the denser surfaces, $\sigma_\theta = 27.2$ and $\sigma_2 = 36.9$, where although the latitudinal trend in DFe_{TOT} is well reflected in DFe_{PRE}, the preformed component is systematically less than DFe_{TOT} (Figures 3e and 3f). Thus, while the latitudinal trend in DFe_{TOT} is well explained by the ventilation process and the resulting signal in DFe_{PRE} in both basins, the departures between DFe_{TOT} and DFe_{PRE} highlight the role of other source terms in equation (1).

3.2. The Role of Subsurface Dissolved Iron Input

Although DFe_{SED} is weak overall (0.024 ± 0.064 nM and 0.017 ± 0.062 nM in the Atlantic and Pacific, respectively), the sedimentary source has a clear signal in the equatorial undercurrent in both basins (Figures 1c and 2c). On $\sigma_\theta = 26.2$ and 27.2 surfaces in the Atlantic, DFe_{SED} is as important as DFe_{PRE} south of the equator and is relatively strong throughout (Figure 3) due to the strong inputs in the region (e.g., from the Caribbean and Patagonian shelves). A similar pattern is seen in the Pacific but is more localized to the Southern Hemisphere (Figure 3, associated with the Campbell plateau south west of New Zealand [*Boyd et al.*, 2012]). DFe_{SED} is absent on the intermediate water surface due to negligible input at these depths.

At the basin mean scale, the influence of DFe_{HYD} increases from the Atlantic (0.12 ± 0.09 nM) to the Pacific (0.31 ± 0.17 nM) and its zonal distribution reflects the overturning circulation and greater hydrothermal inputs in the Pacific (Figure 1d and 2d) [*Tagliabue et al.*, 2010]. In the Atlantic, DFe_{HYD} becomes more important from the lighter to denser mode waters through to the deeper intermediate waters and from
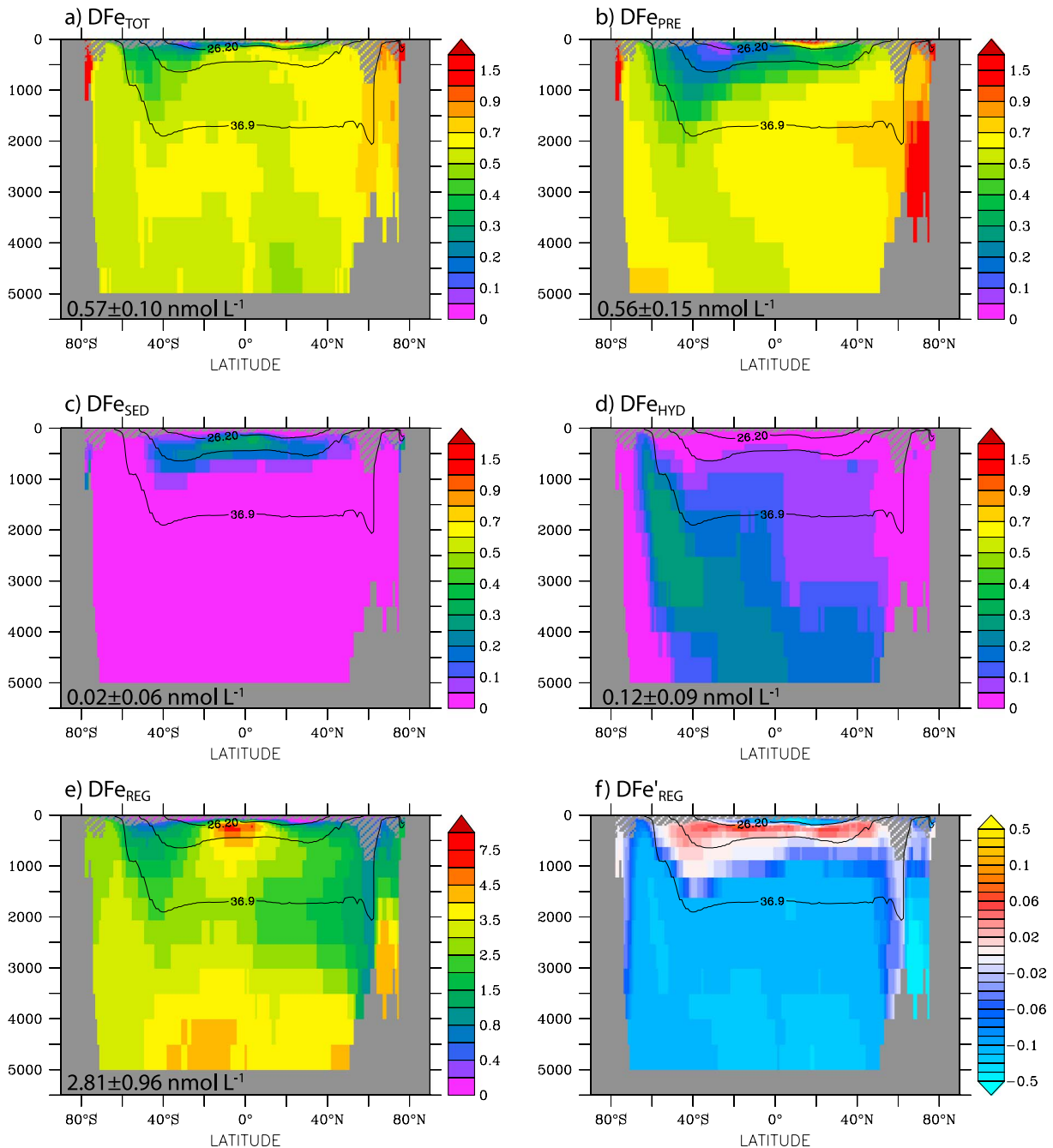
Figure 1. Atlantic Zonal Mean: (a) dissolved Fe (DFe$_{TOT}$, nmol L^{-1}), (b) preformed DFe (DFe$_{PRE}$, nmol L^{-1}), (c) sedimentary DFe (DFe$_{SED}$, nmol L^{-1}), (d) hydrothermal DFe (DFe$_{HYD}$, nmol L^{-1}), (e) regenerated DFe (DFe$_{REG}$, nmol L^{-1}), and (f) net regeneration (DFe'$_{REG}$ = DFe$_{REG}$ − DFe$_{SCAV}$, nmol L^{-1}), where positive values indicate net regeneration and negative values indicate net scavenging. Grey hatched areas denote the zonal mean annual maximum mixed layer depth, and the $\sigma_\theta = 26.2$, 27.2 and $\sigma_2 = 36.9$ isolines are marked.

northerly to southerly latitudes following the overturning circulation (Figure 3). In the Pacific, DFe$_{HYD}$ is prominent on all potential density surfaces due to the larger inputs and the shallower ridges in this basin. Indeed, DFe$_{HYD}$ is almost equal to DFe$_{PRE}$ along the $\sigma_\theta = 27.2$ and $\sigma_2 = 36.9$ surfaces (Figures 3e and 3f).

The effect of the different supply mechanisms on the resulting DFe$_{TOT}$ distribution can be understood by comparing DFe$_{PRE}$ with DFe$_{SED}$ and DFe$_{HYD}$ (Figures 1 and 2). For example, in the Atlantic, DFe$_{SED}$ augments DFe$_{PRE}$ in mode waters, with a similar, but lesser, role played by DFe$_{HYD}$ in south Atlantic intermediate waters. In the Pacific, DFe$_{SED}$ and DFe$_{HYD}$ are similar to DFe$_{PRE}$ in the lightest mode waters (Figure 3d), with their influence
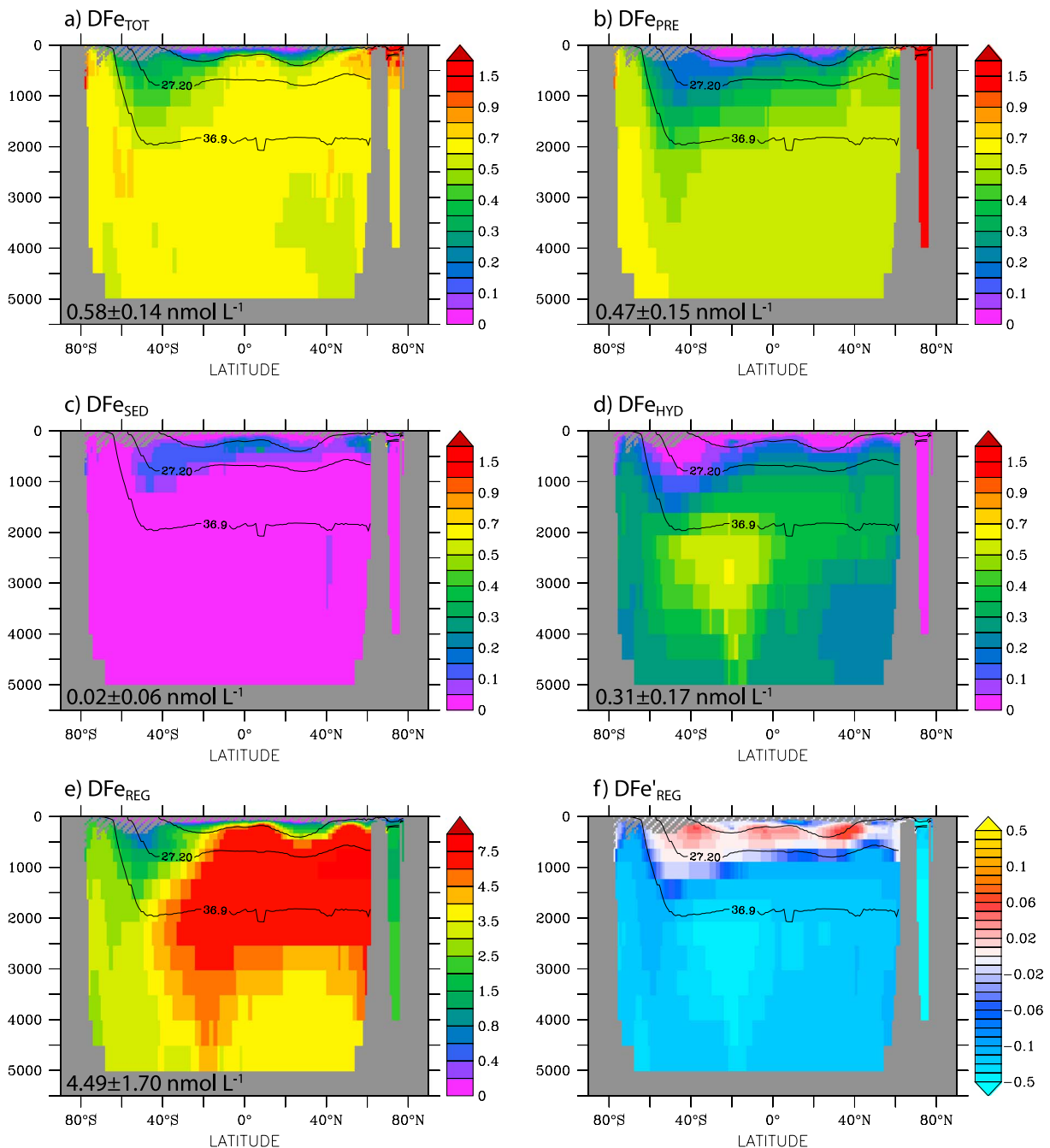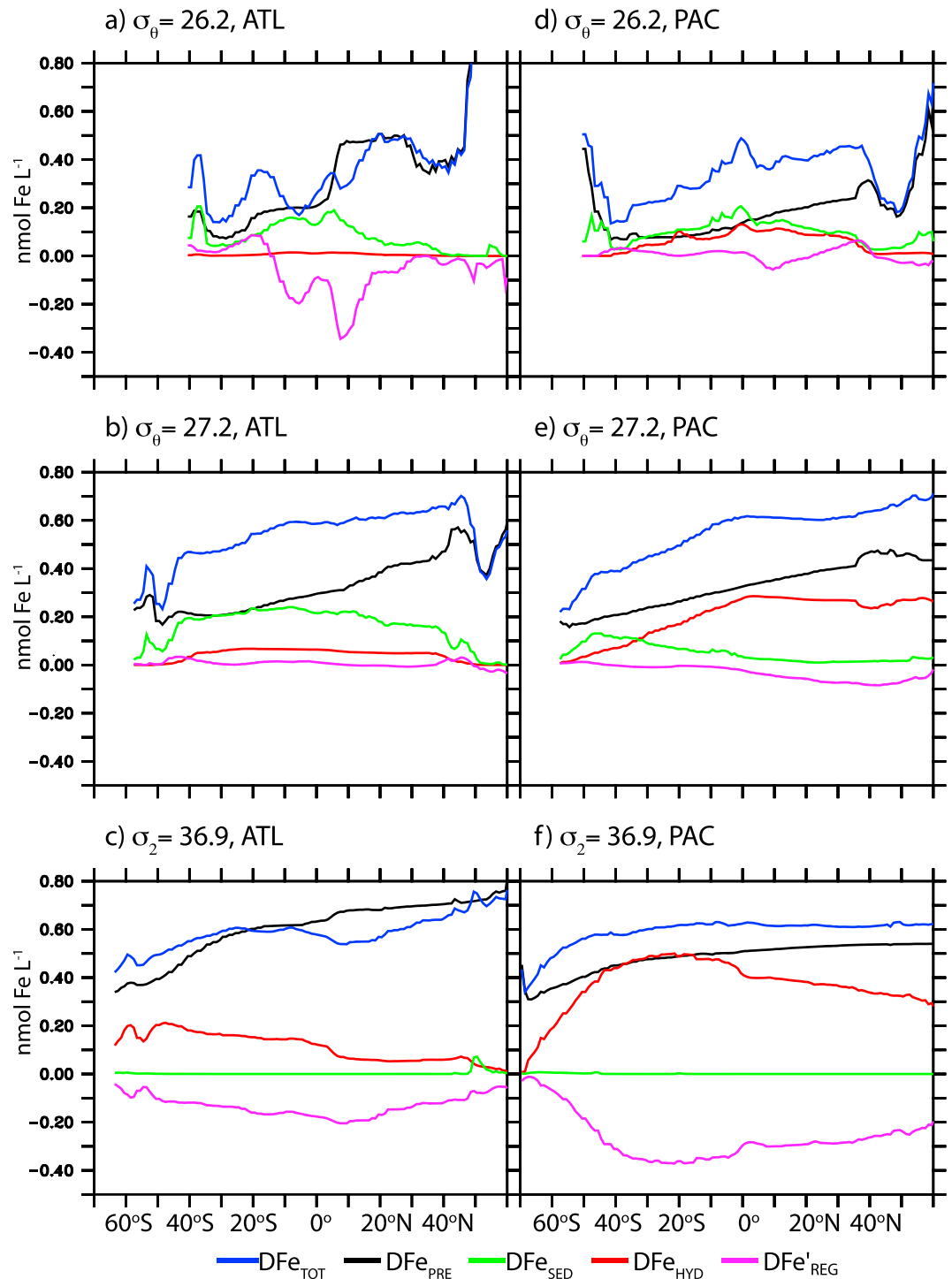
Figure 2. Pacific Zonal Mean: (a) dissolved Fe (DFe$_{TOT}$, nmol L^{-1}), (b) preformed DFe (DFe$_{PRE}$, nmol L^{-1}), (c) sedimentary DFe (DFe$_{SED}$, nmol L^{-1}), (d) hydrothermal DFe (DFe$_{HYD}$, nmol L^{-1}), (e) regenerated DFe (DFe$_{REG}$, nmol L^{-1}), and (f) net regeneration (DFe′$_{REG}$ = DFe$_{REG}$ − DFe$_{SCAV}$, nmol L^{-1}), where positive values indicate net regeneration and negative values indicate net scavenging. Grey hatched areas denote the zonal mean annual maximum mixed layer depth, and the σ_θ = 26.2, 27.2 and σ_2 = 36.9 isolines are marked.

switching from south (DFe$_{SED}$) to north (DFe$_{HYD}$) for the denser mode waters (Figure 3e). Due to strong hydrothermal input associated with the East Pacific Rise [*Tagliabue et al.*, 2010], DFe$_{HYD}$ is as important as DFe$_{PRE}$ in Pacific intermediate waters, highlighting the far-field influence of DFe$_{HYD}$ in this basin [*Wu et al.*, 2011].

3.3. The Regeneration-Scavenging Balance

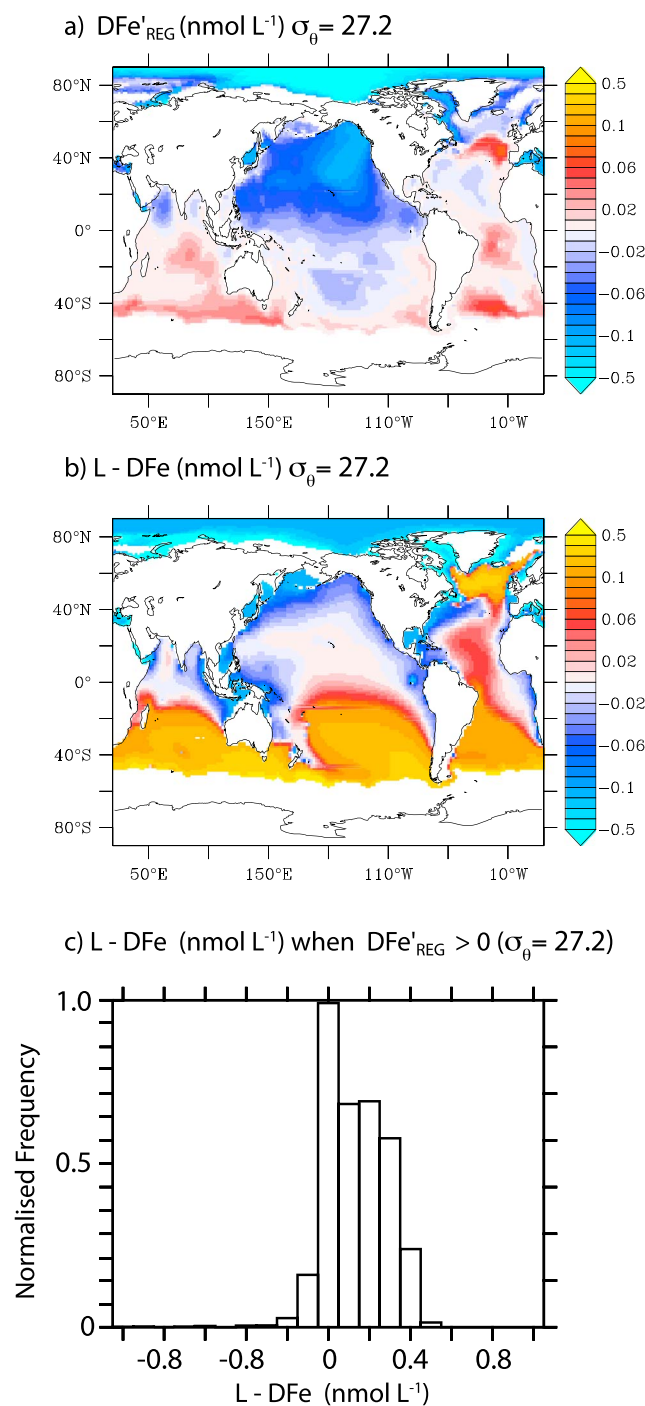The largest terms in equation (1) are associated with DFe$_{REG}$ and DFe$_{SCAV}$, with each term greater in the Pacific than the Atlantic and more or less balancing each other in both basins (DFe$_{REG}$ = 4.49 ± 1.69 nM versus

Figure 3. Zonal Mean for the (a–c) Atlantic and (d–f) Pacific: dissolved Fe (DFe_{TOT}, blue, nmol L^{-1}), preformed DFe (DFe_{PRE}, black, nmol L^{-1}), sedimentary DFe (DFe_{SED}, green, nmol L^{-1}), hydrothermal DFe (DFe_{HYD}, red, nmol L^{-1}), and net regeneration ($DFe'_{REG} = DFe_{REG} - DFe_{SCAV}$, purple, nmol L^{-1}) along $\sigma_\theta = 26.2$ (Figures 3a and 3d), $\sigma_\theta = 27.2$ (Figures 3b and 3e), and $\sigma_2 = 36.9$ (Figures 3c and 3f) surfaces.

$DFe_{SCAV} = 4.71 \pm 1.74$ nM and $DFe_{REG} = 2.81 \pm 0.96$ nM versus $DFe_{SCAV} = 2.94 \pm 1.01$ nM, for Pacific and Atlantic, respectively, Figures 1 and 2 and Figures S1a and S1b in the supporting information). To assess whether this mismatch is simply due to the computation of DFe_{SCAV} as a residual in equation (1), we compare with the actual remineralization and scavenging rates produced by the model: the total remineralization of

a) DFe'$_{REG}$ (nmol L^{-1}) σ_θ = 27.2

b) L - DFe (nmol L^{-1}) σ_θ = 27.2

c) L - DFe (nmol L^{-1}) when DFe'$_{REG}$ > 0 (σ_θ = 27.2)

Figure 4. (a) Net regeneration (DFe'$_{REG}$ = DFe$_{REG}$ − DFe$_{SCAV}$, nmol L^{-1}), (b) the difference between concentrations of ligands and DFe (nmol L^{-1}), both along σ_θ = 27.2 surface and (c) a histogram of the difference between concentrations of ligands and DFe (nmol L^{-1}) at the locations of net regeneration (DFe'$_{REG}$ > 0) on σ_θ = 27.2 surface. The distributions in Figures 4a and 4b reveal a strong ventilated character, consistent with mode water formation and spreading in the high-latitude North Atlantic and Southern Ocean, as well as an absence of ventilation in the North Pacific. Figure 4c shows that waters that encounter net regeneration are typified by greater concentrations of ligands than DFe.

7.56×10^{10} mols yr^{-1} is almost balanced by total scavenging loss of 7.66×10^{10} mols yr^{-1}, which supports our diagnostics of the near cancelation of DFe$_{REG}$ and DFe$_{SCAV}$. It would be interesting to evaluate whether this apparent balance can be assessed from observations.

Despite their opposing contributions and partial cancelation, it is useful to examine the net regeneration-scavenging balance, DFe'$_{REG}$ = DFe$_{REG}$ − DFe$_{SCAV}$, which indicates whether net regeneration (DFe'$_{REG}$ > 0) or net scavenging (DFe'$_{REG}$ < 0) is predominant. On the σ_θ = 26.2 surface, there is a transition from net regeneration to net scavenging from south to north that is stronger in the Atlantic, relative to the Pacific basin (Figures 3a and 3d). In contrast, on the σ_2 = 36.9 surface, there is strong scavenging, larger in the Pacific relative to the Atlantic (Figures 3a and 3f), due to the removal of hydrothermal DFe input. When viewed as zonal means, there is a localized region of net regeneration (DFe'$_{REG}$ > 0) at around 500 m water depth in both basins that is below the σ_θ = 26.2 surface (Figures 1f and 2f). This zone of net regeneration is bracketed at shallow and deeper depths by net scavenging [see also *Boyd and Ellwood*, 2010], where components of the DFe input from hydrothermalism/sediments and regeneration are strongly removed. Understanding this vertical structure is important as it highlights where DFe regeneration is influencing the DFe$_{TOT}$ pool.

A ventilation-based interpretation explains the vertical structure of DFe'$_{REG}$ from a mechanistic standpoint. To illustrate this interpretation, consider the DFe'$_{REG}$ variation along the σ_θ = 27.2 surface for denser subtropical and subpolar mode waters: DFe'$_{REG}$ reveals a clear ventilation imprint, positive values in the well-ventilated mode waters of the southern and northern Atlantic Oceans and negative values in the poorly ventilated waters of the north Pacific (Figure 4a); observations of ventilation tracers, such as CFC-12, dissolved oxygen and radiocarbon, show similar

contrasting patterns for each basin on this surface [*Williams and Follows*, 2011]. In the model, these mode waters are subducted with a large "binding capacity" for DFe as illustrated by the difference between ligand and DFe concentrations (Figure 4b). This term is positive when DFe is low relative to L and indicates extra capacity to stabilize the DFe produced from regeneration. Thus, we propose that when mode waters are subducted with greater concentrations of ligands than DFe, regenerated Fe is retained as DFe, which increases DFe'$_{REG}$ and the overall influence of regeneration. Conversely, if mode waters are subducted with ligand concentrations less than or equal to DFe concentrations then there is no additional binding capacity for DFe, which means that regenerated iron is not retained as DFe and instead is lost by scavenging (decreasing DFe'$_{REG}$). This interpretation is supported by additional diagnostics along the $\sigma_\theta = 27.2$ surface, where regions where DFe'$_{REG}$ is > 0 are overwhelmingly typified by greater concentrations of ligands than DFe (Figure 4c).

In observations, both Southern and Northern mode waters are characterized by excesses in organic ligands [*Ibisanmi et al.*, 2011; *Mohamed et al.*, 2011; *Thuróczy et al.*, 2011], which is largely due to low DFe concentrations at the end of winter [*Ellwood et al.*, 2008; *Nielsdóttir et al.*, 2009; *Tagliabue et al.*, 2012] and is in broad agreement with the model (Figure 4b). Hence, the distribution of DFe'$_{REG}$ along a potential density surface appears to be related to the upstream difference between ligand and DFe concentrations of subducted water, as this controls the vertical distribution of DFe'$_{REG}$. For example, the greater concentrations of ligands than DFe subducted along the mode water surfaces are connected to the discrete zone of net regeneration in Figures 1f and 2f, with net scavenging above and below. The distribution of DFe'$_{REG}$ contrasts with the actual rate of DFe regeneration (Figure S2 in the supporting information), highlighting how little of the total regenerative signal actually influences the DFe pool. This balance is an important contrast with PO$_4$, where regeneration makes up around half of the total PO$_4$ [*Duteil et al.*, 2013]. There are though some regions where the signs of DFe'$_{REG}$ and the difference between ligand and DFe concentrations along the $\sigma_\theta = 27.2$ surface do not match, such as in the South Pacific (Figure 4), which is a consequence of strong scavenging due to benthic DFe sources (both sedimentary and hydrothermal, Figure 3e). In a global sense, there are greater concentrations of ligands than DFe in around 85% of the locations in the model where there is net regeneration, which highlights the importance of the degree of saturation of organic ligands (in terms of DFe) in driving the influence of regeneration on DFe distributions.

4. Implications

4.1. The Importance of Ventilation

Overall, our framework highlights two ways in which ocean ventilation governs the distributions of DFe in the ocean by (1) subducting unused DFe from surface waters as preformed DFe and (2) controlling the regeneration-scavenging balance by subducting waters with distinct ligand-DFe characteristics.

Despite the strong imprint of preformed Fe and ventilation processes in the meridional structure of DFe due to the stabilization of DFe by organic ligands, there are important roles for sediment and hydrothermal DFe sources in the ocean interior. There is a strong, but localized, sedimentary signal in equatorial undercurrent water, as noted from some measurements [*Slemons et al.*, 2010]. Much of the Pacific-Atlantic contrast in DFe$_{HYD}$ is due to the link between DFe and helium input [*Tagliabue et al.*, 2010]. If the Atlantic hydrothermal source has been previously underestimated [*Saito et al.*, 2013], then the magnitude of DFe$_{HYD}$ (but not its trend) should be viewed as a lower bound.

Ultimately, DFe$_{PRE}$, DFe$_{HYD}$, and DFe$_{SED}$ form a backdrop onto which regenerated DFe operates. The degree of ventilation and difference between ligand and DFe concentrations of a given water parcel dictates how strongly the regeneration signal is seen in the DFe concentration that would be measured. If there is little ligand binding capacity for DFe in a subducted water parcel (either due to preformed, sedimentary, hydrothermal, or even DFe that is desorbed from particles), then there will be no imprint of regeneration. In contrast, only when excess ligands are present is a regeneration signal seen in DFe$_{TOT}$. The variability in DFe'$_{REG}$ will complicate attempts to determine Fe/C ratios of sinking particles from correlations of AOU and DFe$_{TOT}$ from field measurements [*Fitzsimmons et al.*, 2013; *Rijkenberg et al.*, 2012] as the precise contribution of DFe$_{REG}$ can range widely (e.g., Figures 1f and 2f). We suggest that variations in ventilation and/or the balance between ligand and DFe concentrations can make DFe regeneration a stronger or weaker

component of the ocean inventory of DFe in different places and times. Although our model uses a fixed ligand concentration (0.6 nM), we expect that employing a model of dynamic ligand concentrations would not modify the importance of ligand saturation for the downstream DFe distribution as the concentration of ligands would only increase. However, it would be interesting to examine how the production of ligands [*Boyd et al.*, 2010] during regeneration affects DFe'$_{REG}$.

4.2. Application to Observations

In recent years, field observations of DFe have increased markedly with substantial data sets available from ocean sections as part of the GEOTRACES program (www.geotraces.org). Despite this wealth of data, ascribing a particular process to an observed feature remains difficult due to the interacting influences of DFe$_{PRE}$, DFe$_{HYD}$, DFe$_{SED}$, DFe$_{REG}$, and DFe$_{SCAV}$, which can overlap and compensate for each other (Figures 1 and 2). Our framework (section 2) is able to quantify their different roles in our model, and ultimately applying it to field data will allow us to illuminate important aspects of the Fe cycle if the different terms can be constrained. For example, in situ measurements of the Fe content of sinking particles [*Twining et al.*, 2014] alongside AOU can produce DFe$_{REG}$; although subduction of undersaturated O$_2$ can lead to an error in this estimation [*Duteil et al.*, 2013]. As DFe$_{PRE}$ is tied to the end-member surface DFe concentration, observations of end of winter DFe in outcrop regions for the $\sigma_\theta = 27.2$ and $\sigma_2 = 36.9$ surfaces (North Atlantic and Southern Ocean) could allow DFe$_{PRE}$ to be diagnosed, as suggested for preformed O$_2$ [*Duteil et al.*, 2013]. Coincidence between DFe and helium is often used to highlight hydrothermal influence on DFe [*Saito et al.*, 2013; *Wu et al.*, 2011], and if source signatures are obtained, this approach may constrain DFe$_{HYD}$. Finally, determining DFe$_{SED}$ may require novel use of sediment specific tracers such as manganese [*Slemons et al.*, 2010], radium isotopes [*Charette et al.*, 2007], or neodymium isotopes [*Lacan and Jeandel*, 2005].

5. Conclusions

We have described a new ventilated framework to delineate the different contributions of the subduction of unused surface DFe, subsurface DFe inputs, DFe regeneration, and scavenging to the distributions of DFe in a global ocean model. While the subsurface DFe distribution might be expected to simply reflect the effect of surface and benthic sources, our model finds a strong effect of ventilation and circulation. The subduction of preformed DFe and the difference between ligand and DFe concentrations play an important role in governing the distributions of DFe and the regeneration-scavenging balance in the ocean interior. Unlike for PO$_4$, there is a strong partial cancelation between the regeneration and scavenging of DFe in our model. The remaining regions of net regeneration at depth correspond with potential density surfaces where there is upstream subduction of waters with greater concentrations of ligands than DFe. Ultimately, our framework and model diagnostics highlight the competing influences of local sources versus ventilation and circulation in controlling the distribution of DFe. With suitable further development, our framework may be applied to field observations to reveal the local and far-field control of the ocean Fe cycle.

References

Boyd, P. W., and M. J. Ellwood (2010), The biogeochemical cycle of iron in the ocean, *Nat. Geosci.*, *3*(10), 675–682, doi:10.1038/ngeo964.

Boyd, P. W., E. Ibisanmi, S. G. Sander, K. A. Hunter, and G. A. Jackson (2010), Remineralization of upper ocean particles: Implications for iron biogeochemistry, *Limnol. Oceanogr.*, *55*(3), 1271–1288, doi:10.4319/lo.2010.55.3.1271.

Boyd, P. W., K. R. Arrigo, R. Strzepek, and G. L. van Dijken (2012), Mapping phytoplankton iron utilization: Insights into Southern Ocean supply mechanisms, *J. Geophys. Res.*, *117*, C06009, doi:10.1029/2011JC007726.

Charette, M. A., M. E. Gonneea, P. J. Morris, P. Statham, G. Fones, H. Planquette, I. Salter, and A. N. Garabato (2007), Radium isotopes as tracers of iron sources fueling a Southern Ocean phytoplankton bloom, *Deep Sea Res., Part II*, *54*(18–20), 1989–1998, doi:10.1016/j.dsr2.2007.06.003.

Duteil, O., et al. (2012), Preformed and regenerated phosphate in ocean general circulation models: Can right total concentrations be wrong?, *Biogeosciences*, *9*(5), 1797–1807, doi:10.5194/bg-9-1797-2012.

Duteil, O., W. Koeve, A. Oschlies, D. Bianchi, E. Galbraith, I. Kriest, and R. Matear (2013), A novel estimate of ocean oxygen utilisation points to a reduced rate of respiration in the ocean interior, *Biogeosciences*, *10*(11), 7723–7738, doi:10.5194/bg-10-7723-2013.

Ellwood, M. J., P. W. Boyd, and P. Sutton (2008), Wintertime dissolved iron and nutrient distributions in the Subantarctic Zone from 40–52S; 155–160E, *Geophys. Res. Lett.*, *35*, L11604, doi:10.1029/2008GL033699.

Fitzsimmons, J. N., R. Zhang, and E. A. Boyle (2013), Dissolved iron in the tropical North Atlantic Ocean, *Mar. Chem.*, *154*, 87–99, doi:10.1016/j.marchem.2013.05.009.

Hanawa, K., and L. D. Talley (2001), Mode waters, in *Ocean Circulation and Climate: Observing and Modelling the Global Ocean*, edited by G. Siedler, J. Church, and J. Gould, pp. 373–386, Academic Press, San Diego, Calif.

Ibisanmi, E., S. G. Sander, P. W. Boyd, A. R. Bowie, and K. A. Hunter (2011), Vertical distributions of iron-(III) complexing ligands in the Southern Ocean, *Deep Sea Res., Part II*, *58*(21–22), 2113–2125, doi:10.1016/j.dsr2.2011.05.028.

Ito, T., and M. J. Follows (2005), Preformed phosphate, soft tissue pump and atmospheric CO_2, *J. Mar. Res.*, *63*(4), 813–839, doi:10.1357/0022240054663231.

Jickells, T. D., et al. (2005), Global iron connections between desert dust, ocean biogeochemistry, and climate, *Science*, *308*(5718), 67–71, doi:10.1126/Science.1105959.

Lacan, F., and C. Jeandel (2005), Neodymium isotopes as a new tool for quantifying exchange fluxes at the continent–ocean interface, *Earth Planet. Sci. Lett.*, *232*(3–4), 245–257, doi:10.1016/j.epsl.2005.01.004.

Mohamed, K. N., S. Steigenberger, M. C. Nielsdottir, M. Gledhill, and E. P. Achterberg (2011), Dissolved iron (III) speciation in the high latitude North Atlantic Ocean, *Deep Sea Res., Part I*, *58*(11), 1049–1059, doi:10.1016/j.dsr.2011.08.011.

Moore, C. M., et al. (2013), Processes and patterns of oceanic nutrient limitation, *Nat. Geosci.*, doi:10.1038/ngeo1765.

Nielsdóttir, M. C., C. M. Moore, R. Sanders, D. J. Hinz, and E. P. Achterberg (2009), Iron limitation of the postbloom phytoplankton communities in the Iceland Basin, *Global Biogeochem. Cycles*, *23*, GB3001, doi:10.1029/2008GB003410.

Rijkenberg, M. J. A., S. Steigenberger, C. F. Powell, H. van Haren, M. D. Patey, A. R. Baker, and E. P. Achterberg (2012), Fluxes and distribution of dissolved iron in the eastern (sub-) tropical North Atlantic Ocean, *Global Biogeochem. Cycles*, *26*, GB3004, doi:10.1029/2011GB004264.

Saito, M. A., A. E. Noble, A. Tagliabue, T. J. Goepfert, C. H. Lamborg, and W. J. Jenkins (2013), Slow-spreading submarine ridges in the South Atlantic as a significant oceanic iron source, *Nat. Geosci.*, doi:10.1038/ngeo1893.

Schlosser, C., J. K. Klar, B. D. Wake, J. T. Snow, D. J. Honey, E. M. Woodward, M. C. Lohan, E. P. Achterberg, and C. M. Moore (2013), Seasonal ITCZ migration dynamically controls the location of the (sub)tropical Atlantic biogeochemical divide, *Proc. Natl. Acad. Sci. U.S.A.*, doi:10.1073/pnas.1318670111.

Slemons, L. O., J. W. Murray, J. Resing, B. Paul, and P. Dutrieux (2010), Western Pacific coastal sources of iron, manganese, and aluminum to the Equatorial Undercurrent, *Global Biogeochem. Cycles*, *24*, GB3024, doi:10.1029/2009GB003693.

Strzepek, R. F., K. A. Hunter, R. D. Frew, P. J. Harrison, and P. W. Boyd (2012), Iron-light interactions differ in Southern Ocean phytoplankton, *Limnol. Oceanogr.*, *57*(4), 1182–1200, doi:10.4319/lo.2012.57.4.1182.

Tagliabue, A., et al. (2010), Hydrothermal contribution to the oceanic dissolved iron inventory, *Nat. Geosci.*, *3*(4), 252–256, doi:10.1038/ngeo818.

Tagliabue, A., T. Mtshali, O. Aumont, A. R. Bowie, M. B. Klunder, A. N. Roychoudhury, and S. Swart (2012), A global compilation of dissolved iron measurements: Focus on distributions and processes in the Southern Ocean, *Biogeosciences*, *9*(6), 2333–2349, doi:10.5194/bg-9-2333-2012.

Tagliabue, A., O. Aumont, and L. Bopp (2014a), The impact of different external sources of iron on the global carbon cycle, *Geophys. Res. Lett.*, *41*, 920–926, doi:10.1002/2013gl059059.

Tagliabue, A., J.-B. Sallée, A. R. Bowie, M. Lévy, S. Swart, and P. W. Boyd (2014b), Surface-water iron supplies in the Southern Ocean sustained by deep winter mixing, *Nat. Geosci.*, *7*, 314–320, doi:10.1038/ngeo2101.

Talley, L. D. (1999), Some aspects of ocean heat transport by the shallow, intermediate and deep overturning circulations, in *Mechanisms of Global Climate Change at Millennial Time Scales, Geophys. Monog. Ser.*, vol. 112, edited by P. U. Clark, R. S. Webb, and L. D. Keigwin, pp. 1–22, AGU, Washington, D. C., doi:10.1029/GM112p0001.

Thuróczy, C. E., L. J. A. Gerringa, M. B. Klunder, P. Laan, and H. J. W. de Baar (2011), Observation of consistent trends in the organic complexation of dissolved iron in the Atlantic sector of the Southern Ocean, *Deep Sea Res., Part II*, *58*(25–26), 2695–2706, doi:10.1016/j.dsr2.2011.01.002.

Twining, B. S., S. D. Nodder, A. L. King, D. A. Hutchins, G. R. LeCleir, J. M. DeBruyn, E. W. Maas, S. Vogt, S. W. Wilhelm, and P. W. Boyd (2014), Differential remineralization of major and trace elements in sinking diatoms, *Limnol. Oceanogr.*, *59*(3), 689–704, doi:10.4319/lo.2014.59.3.0689.

Ussher, S. J., E. P. Achterberg, C. Powell, A. R. Baker, T. D. Jickells, R. Torres, and P. J. Worsfold (2013), Impact of atmospheric deposition on the contrasting iron biogeochemistry of the North and South Atlantic Ocean, *Global Biogeochem. Cycles*, *27*, 1096–1107, doi:10.1002/gbc.20056.

Williams, R. G., and M. J. Follows (2011), *Ocean Dynamics and the Carbon Cycle: Principles and Mechanisms*, Cambridge Univ. Press, Cambridge, U. K.

Wu, J., M. L. Wells, and R. Rember (2011), Dissolved iron anomaly in the deep tropical–subtropical Pacific: Evidence for long-range transport of hydrothermal iron, *Geochim. Cosmochim. Acta*, *75*(2), 460–468, doi:10.1016/j.gca.2010.10.024.